ISSN 1087-6596, Glass Physics and Chemistry, 2023, Vol. 49, No. 2, pp. 150–159. © Pleiades Publishing, Ltd., 2023.

Silicon Oxide Modified with Gadolinium and Europium Oxides – Synthesis, Properties and Application Prospects

S. I. Niftaliev[a], I. V. Kuznetsova[a, *], I. A. Zvereva[b], L. V. Lygina[a], A. A. Sinelnikov[c], I. A. Saranov[d], K. B. Kim[a], and S. S. Chernenko[a]

[a] *Department of Inorganic Chemistry and Chemical Technology, Voronezh State University of Engineering Technologies, Voronezh, 394036 Russia*

[b] *Institute of Chemistry, St. Petersburg State University, St. Petersburg, 199034 Russia*

[c] *Center for the Collective Use of Scientific Equipment, Voronezh State University, Voronezh, 394018 Russia*

[d] *Department of Information Security, Voronezh State University of Engineering Technologies, Voronezh, 394036 Russia*

**e-mail: kuznetsovaiv@mail.ru*

Received August 29, 2022; revised October 10, 2022; accepted December 12, 2022

Abstract—The SiO_2, Gd_2O_3–SiO_2 and Eu_2O_3–SiO_2 were synthesized by two ways – using the silicon oxide isolated from kaolin and using the silicon oxide obtained by hydrolysis of tetraethoxysilane. Agar-agar (polysaccharide) was added as a structure-forming agent and the freeze-drying was used for obtaining powders. DSC and TG up to 700°C revealed endothermic effects corresponding to the loss of free moisture, the decomposition of metal hydroxide and hydroxogroups (≡Si–OH) from the silica surface. The powders calcined at 700°C are X-ray amorphous. The morphology of the samples was studied using transmission electron microscopy (TEM) and dynamic light scattering (DLS). The hydrodynamic size of the particles synthesized from kaolin, determined using DLS method, exceeds the particle size established by TEM. The hydrodynamic size of the nanoparticles obtained from tetraethoxysilane is within the particle size determined by TEM. The agglomerates formed by particles synthesized from tetraethoxysilane are less strong than those obtained from kaolin. In the Eu_2O_3–SiO_2 system-based composition obtained using tetraethoxysilane, nanocrystallinity with a particle size of 8–40 nm was detected. The luminescence excitation spectra for the Eu_2O_3–SiO_2 samples syn-thesized by both ways differ in the ratio of the supersensitive $^5D_0$–$^7F_2$ and magnetodipole $^5D_0$–$^7F_1$ transition bands. For the Gd_2O_3–SiO_2 nanopowder obtained from tetraethoxysilane, an increase in the $^5D_0$–$^7F_2$ inten-sity, as well as the appearance of a second $^5D_0$–$^7F_1$ peak were observed.

Keywords: silicon oxide, gadolinium oxide, europium oxide, kaolin, tetraethoxysilane

DOI: 10.1134/S108765962260096X

INTRODUCTION

The synthesis and study of mesoporous mesophase silicate materials (MSNs), as well as metal composites based on them, are continuously gaining attention of many researchers. Due to their unique properties (high specific surface area more than 1000 m^2/g, large pore volume up to 2 cm^3/g, nanodispersity) and long-range order structure (in contrast to the well-known silica gels and aerogels) MSNs have already found wide application in the processes of selective sorption [1, 2], catalysis [3, 4], and as nanoreactors [5, 6] for the synthesis of various materials. Promising directions are related to the use of MSNs as optical biosensors [7, 8] and the development of a new generation of drugs for targeted delivery of the active substance to specific areas of the body [9, 10].

The methods for synthesizing silicate materials are also diverse [11]. Mesoporous silicon oxide can be obtained from TEOS (tetraethyl orthosilica) and RH (Rise husk) [11]. The authors [12] synthesize mesoporous polymetallic silicate from red clay. In [13] the silicon/reduced graphene oxide (Si/rGO) was synthesized from clay. The structural features make mesoporous Si/rGO a very suitable anode material for lithium-ion batteries. Mesoporous silicon oxide was synthesized from iron ore tailings by fusion with alkali followed by acid leaching [14]. The obtained samples have a specific surface area up to 544.68 m^2/g of irregular mesoporous structure; they show good adsorption properties with respect to the methylene blue dye (maximum adsorption capacity corresponded to 192 mg/g). In [15] bimodal silica particles of nanometer and micrometer size were obtained from bentonite clay, which was subjected to thermal and acid treatment to reduce the alumina content and increase the amount of silica.

The presence of reactive silanol groups (≡ Si–OH) [16] on the surface of silica particles makes it possible to modify them using various methods [17, 18], regu-

late their electrosurface properties [19], aggregative stability, porous structure [20], and obtain compounds with a wide range of applications [21, 22]. The authors [23] determined the amount of sobbed water and silanol groups on the silica surface by thermogravimetric analysis. A large number of silanol groups reduce the cohesion of the silica-oxygen framework of the material, and hence its stability.

Metal oxide compositions (metal oxide – silicon oxide) can be obtained using various methods: coprecipitation (copolycondensation) of metal oxide with the base material, by impregnation – intercalation of metal oxides in a previously synthesized matrix and by various combinations of these methods [24–26]. Ultimately, a variety of composites different from the structure of the siloxane skeleton and the nature of the introduced metal atom are formed. The synthesis methods developed so far make it possible to obtain both individual framework compounds and oligomeric metalorganosiloxanes [27, 28].

The gadolinium oxide – mesoporous silicon dioxide system (Gd–MS) can be used as an alternative for the synthesis of contrast agents for magnetic resonance imaging (MRI) [29]. MRI mainly uses chelated gadolinium compounds, which are toxic and accumulate in tissues. Nanodispersed gadolinium silicates are less toxic and remain in the bloodstream longer. The higher content of gadolinium in the silicate than in the chelate complexes will increase the sensitivity and reduce the dosage of these drugs. In [29], Gd–MS was prepared using a sol-gel method. The particles are nanosized and can easily penetrate the cell.

In [30] the authors obtained mesoporous amorphous-crystalline SiO_2 and SiO_2–Gd_2O_3 nanopowders (NPs) by pulsed electron beam evaporation (PEBE). Phase analysis showed amorphous and three crystalline phases in the Gd_2O_3 nanopowder. The effect of silicon oxide doping on the textural, magnetic, and luminescent properties of Gd_2O_3–SiO_2 NPs was studied. The size and volume of interparticle pores of Gd_2O_3–SiO_2 NPs depended on the dopant content contributed to an increase in amorphousness and the concentration of various structural defects. Annealing and doping led to the degradation of the Gd_2O_3 matrix crystallinity. The correlation of concentration dependence of porosity, paramagnetic response, and intensity of pulsed cathodoluminescence spectra in Gd_2O_3–SiO_2 NPs was established.

Among the rare-earth elements, europium stands out, because it has a long lifetime of excited states and emission in the visible part of the spectrum, which determines the prospects of its use for the diagnosis of various diseases. Red and blue solid luminescent nanopowder due to the presence of the Eu^{3+}/Eu^{2+} ions in the SiO_2 matrix has been successfully synthesized using sol-gel method by drying the precursor gels at room temperature followed by annealing at 500 and 1000°C in ambient air [31]. The phase and morphology of the nanopowder were determined by X-ray diffraction, Fourier transform infrared spectroscopy (FTIR), and transmission electron microscopy (TEM). The transformation of europium oxide from the amorphous phase to the monoclinic phase was observed as a result of annealing, and its effect on the optical properties studied by UV spectroscopy and photoluminescence (PL) are discussed in detail. A red shift was observed at the edge of the absorption band due to annealing, and the bandgap energy also decreased. Luminescent Eu^{3+} species in a silica matrix exhibit intense red emission at 614 nm.

The aim of this work is to synthesize systems Gd_2O_3–SiO_2 and Eu_2O_3–SiO_2, to study the morphology and thermodestruction processes of the obtained materials, to determine their luminescent properties. This study has been performed with the prospect of creating the ternary systems Gd_2O_3–Eu_2O_3–SiO_2, which can be used in medicine for opti-cal imaging simultaneously with MRI [32].

MATERIALS AND METHODS

For the synthesis, as the initial components nitrates $Gd(NO_3)_3 \cdot 6H_2O$, and $Eu(NO_3)_3 \cdot 5H_2O$ (chemically pure), ammonium hydroxide $NH_3 \cdot H_2O$ (chemically pure), crystalline agar-agar (Denagar 900 GA), kaolin (PLAST-RIFEY), and tetraethoxysilane have been used.

The systems SiO_2, Gd_2O_3–SiO_2, Eu_2O_3–SiO_2 were synthesized by two ways according to Scheme 1 and Scheme 2 (Fig. 1).

Scheme 1. SiO_2 was obtained from kaolin. Its sample was fused with sodium and potassium carbonates at 900°C, then obtained alloy was leached with hydro-chloric acid. The white precipitate was washed with water, dried, and calcined at 1000°C. The calcined SiO_2 was loaded into the chemical reactor, water and 1% agar-agar solution were added, 0.1 M solutions of gadolinium (or europium) nitrate and ammonium hydroxide were added dropwise under stirring. The obtained gels were washed, freeze-dried, and calcined at 750°C for 4 h.

The obtained by Scheme 1 samples were designated as following: SiO_2 isolated from kaolin – Sik, SiO_2 modified with Gd_2O_3 – SikGd, SiO_2 modified with Eu_2O_3 – SikEu.

Scheme 2. SiO_2 was obtained by hydrolysis of tetraethoxysilane in ammonia solution. For this purpose, tetraethoxysilane solution was mixed with gadolinium (or europium) nitrates and 1% agar-agar solution was added. The mixture with all components was heated to 70°C with continuous stirring for 2 h. The resulting gel was dried at 105°C for 3 h, then washed with water to a neutral medium and calcined for 4 h at 750°C.

The obtained by Scheme 2 samples were designated as following: SiO_2 isolated from tetraethoxysi-

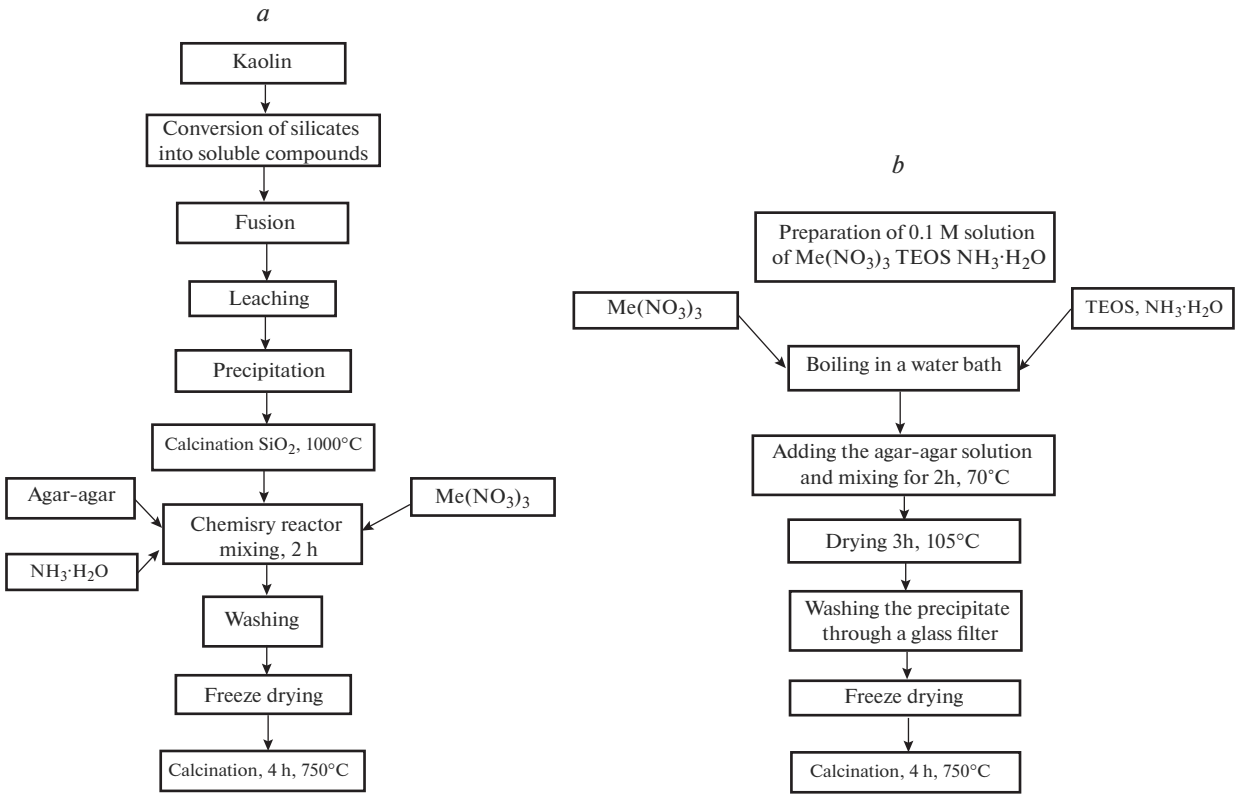

Fig. 1. Two schemes of the synthesis of SiO_2, Gd_2O_3–SiO_2 and Eu_2O_3–SiO_2: (a) using SiO_2 from kaolin, (b) using SiO_2 obtained by hydrolysis of tetraethoxysilane (TEOS).

lane – Sit, SiO_2 modified with Gd_2O_3 – SitGd, SiO_2 modified with Eu_2O_3 – SitEu.

Thermodestruction processes were studied by thermogravimetry (TG) and differential scanning calorimetry (DSC) using NETZSCH STA 449 F3 Jupiter simultaneous thermal analyzer in platinum crucibles. The samples were heated in a nitrogen atmosphere to 1000 °C at a rate of 5 K/min. The temperature measurement error ±1.5 %. Discreteness of indications of loss of weight 0.025 mkg.

The structure of the sample was examined using a transmission electron microscopy (TEM) using ZEISS Libra 120 microscope. Samples of nanopowder for TEM study were prepared as follows: grids with a thin film of amorphous carbon were dipped into the powder suspension with gelatin solution. The excess liquid was removed using ashless filter paper.

The particle size was determined by dynamic light scattering (DLS) on a Malvern Zetasizer Nano ZSP spectrophotometer with noninvasive backscattering optics (NIBS). An aqueous suspension of the non-water-soluble powders was prepared by sonication treatment with the emitter frequency of 20 kHz for 5 min on the SONICATOR Q500 ultrasonic disperser. 2 ml of aqueous suspension of the tested material after ultrasonic treatment was placed in a translucent cuvette. Chemical and elemental composition was deter-mined using a wave X-ray fluorescence spectrometer Bruker S8 Tiger. The accelerating voltage was 60 kV, Bruker Quant Express technique for non-standard analysis of chemical elements have been used.

The phase composition was determined by powder X-ray diffraction analysis in a monocrystalline silicon cuvette using diffractometer Bruker D2 PHASER (Cu Kα radiation).

Diffraction spectrophotometer Ocean Optics USB2000+XR1 was used to measure the photolumi-nescence spectra in the range of 200–900 nm. Semi-conductor LED module High Power Lighting-H77GV1BT-V1 with radiation wavelength 380 nm and laser module Osram LD PL-TB450 with radiation wavelength 445 nm were used as excitation sources. For the measuring the photoluminescence spectra the suspension was deposited on a clean quartz substrate and dried.

RESULTS AND DISCUSSION

Synthesis of Materials

During the fusion of kaolin with carbonates according to Scheme 1 (Fig. 1a) a mixture of alkaline silicates and aluminates is formed:

$$Al_2O_3 \cdot 2SiO_2 \cdot 2H_2O + 3Na_2CO_3 \rightarrow 2Na_2O \cdot SiO_2 + Na_2O \cdot Al_2O_3 + 3CO_2 + 2H_2O. \quad (1)$$

Table 1. Results of the thermal analysis (DSC and TG) of samples after freeze drying

Sample	1st endothermal effect		2nd endothermal effect		3d endothermal effect		Overall mass loss, %
	temperature interval, °C DSC	mass loss, %	temperature interval, °C DSC	mass loss, %	temperature interval, °C DSC	mass loss, %	
SikGd	30–150 (peak 80.8)	12.4	310–500 (peak 423.4)	7.41	–		19.81
SikEu	25–150 (peak 79.4)	12.52	350–500 (peak 417.2)	7.45	–		19.97
SitGd	25–145 (peak 86.4)	12.60	340-490 (peak 400.2)	7.45	620–700 (peak 684.8)	2.57	22.62
SitEu	25–140 (peak 88.6)	12.58	345–500 (peak 400.3)	7.45	628–695 (peak 676.4)	3.53	23.56

Leaching of the alloy with hydrochloric acid leads to the formation of a white precipitate H_2SiO_3:

$$Na_2O \cdot SiO_2 + 2HCl \rightarrow H_2SiO_3 + 2NaCl. \quad (2)$$

Calcination results in the loss of water in silicic acid:

$$H_2SiO_3 \rightarrow SiO_2 + H_2O. \quad (3)$$

The resulting silicon oxide interacts with metal hydroxides obtained from nitrates:

$$Me(NO_3)_3 + 3NH_3 \cdot H_2O \rightarrow Me(OH)_3 + 3NH_4NO_3, \quad (4)$$

$$2Me(OH)_3 + SiO_2 \rightarrow Me_2O_3 \cdot SiO_2 + 3H_2O, \quad (5)$$

where Me = Gd or Eu.

The chemical processes occurring according to the Scheme 2 (Fig. 1b) can be described by the following equations:

$$Si(OC_2H_5)_4 + 4H_2O \rightarrow Si(OH)_4 + 4C_2H_5OH, \quad (6)$$

$$Me(NO_3)_3 + 3NH_3 \cdot H_2O \rightarrow Me(OH)_3 + 3NH_4NO_3, \quad (7)$$

$$2Me(OH)_3 + Si(OH)_4 \rightarrow Me_2O_3 \cdot SiO_2 + 5H_2O. \quad (8)$$

As a result of the synthesis according to both schemes the gel-like products were obtained. During the evaporation of liquid from gel, the capillary pressure arising in small pores can become great. For example, in pores of size 1 nm, a pressure of the order of 1.5×10^8 Pa occurs [33]. As a rule, the presence of some pore size distribution leads to the collapse of the porous structure. Therefore, to maintain gel integrity, it is necessary to minimize either the pressure drop or the capillary pressure itself. One way of minimizing the capillary pressure is to add organic molecules that resist drying by a more uniform pressure distribution in the gel structure [33]. For the production of ceramics different gelling agents of inorganic and organic nature (gelatin, agar, agarose, carrageenan, etc.) have been used [34, 35]. In [35] the authors used agar-agar as a structure-forming agent retaining water in its structure during drying of gadolinium oxide gel. In this study during the synthesis according to both schemes we added agar-agar (polysaccharide) which retains its gelling properties within a wide pH range.

Freeze drying is used in both schemes. This type of drying has a significant impact on the nanostructure of products, their characteristics, the possibility of further processing, and stability during storage [36].

Thermal Analysis

The results of the investigation of thermal destruction processes of the samples obtained after freeze drying by thermal analysis (TG and DSC) are presented in Table 1 and Fig. 2.

The DSC curves of the SikGd and SikEu samples obtained by Scheme 1 (Fig. 2a) after freeze drying revealed two endothermic effects with close values of temperature and mass loss. The first effect (25–150°C) corresponds to the loss of free moisture, the second one (310–500°C) – to the decomposition of metal hydroxide on the surface of silicon oxide by reaction (5), in this temperature range the removal of agar-agar also occurs.

The samples SitGd, SitEu obtained according to the Scheme 2 (Fig. 2b) after freeze drying demonstrates the lose mass in three steps: the first corresponds to the loss of free moisture, the second to the decomposition of metal hydroxide and silicon hydroxide by reaction (8) and the removal of agar-agar, the third (620–700°C) to the removal of the remaining hydroxogroups (≡ Si–OH) unbound to metal atoms from the silica surface. The higher total mass loss (22.62 and 23.56%) compared to the mass loss of the samples obtained according to the Scheme 1 (19.81 and 19.97) indicates moisture retention in the silicon oxide structure. The difference in mass loss of the

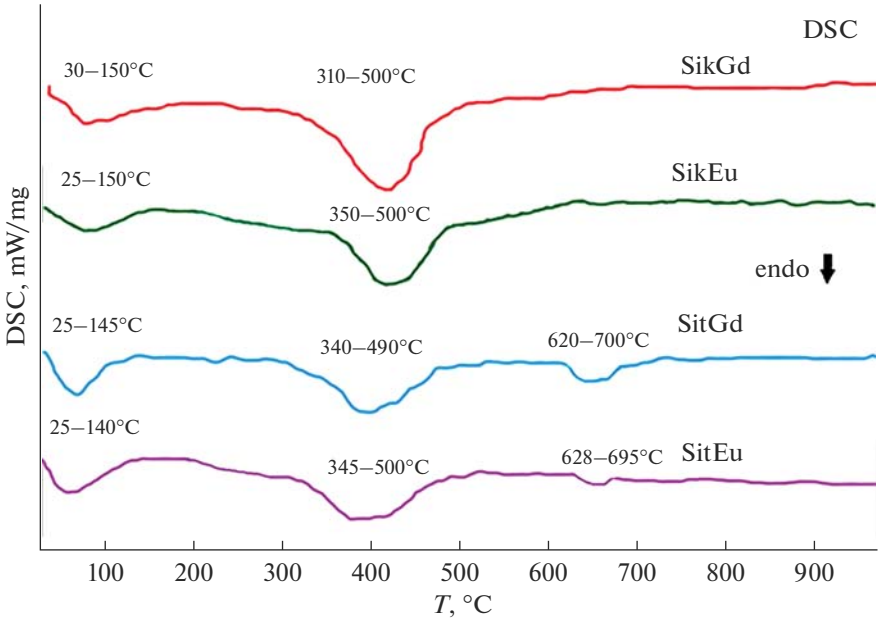

Fig. 2. DSC curves for the samples after freeze drying.

samples obtained according to different schemes ~3–4% (Table 2), which approximately corresponds to the content of hydroxyl groups in mesoporous silica [23]. The change in mass occurs up to 700°C. No peaks of exothermic effects, which may correspond to the crystallization of monoclinic europium oxide, europium or gadolinium silicates, or other processes up to 1000°C, were detected in DSC curves.

Phase Analysis and Composition

X-ray phase study of the samples calcined at 700°C showed that all systems are X-ray amorphous – there were no diffraction peaks on the X-ray patterns. However, in the systems SiO_2–Gd_2O_3 and SiO_2–Eu_2O_3 heated to 1000°C the formation of crystalline hydroxides, rare-earth oxides, as well as their polymorphic transformations were noted [30, 31]. So, we can presume that some conditions in the technology chosen in this study constrain the crystallization processes. For example, agar-agar and freeze drying are used in both diagrams. Presumably, the retention of water in the agar-agar structure and its gradual release during heating keeps the amorphous phase of the systems longer and prevents the crystallization of the products.

The chemical and elemental composition of samples after calcination showed their purity – there are only the elements Si, Gd, Eu, O in stoichiometric ratios to form oxides with proper formula (third column in Table 2). For example, for the sample Sit, the mass ratio Si : O = 46.7 : 53.3%, which corresponds to SiO_2. For the sample SitGd, the mass ratio Si : O : Gd = 42.1 : 49.3 : 8.6%, corresponding to the formation of SiO_2–Gd_2O_3.

Table 2. Content and particle size of the samples obtained according to Scheme 1 and Scheme 2

Method of synthesis	Sample	Formula	Particle size, nm	
			TEM	Peak DLS
Scheme 1	Sik amorphous	SiO_2	200–270	450
	SikGd amorphous	SiO_2–Gd_2O_3	60–270	59 460
	SikEu amorphous	SiO_2–Eu_2O_3	200–700	830
Scheme 2	Sit amorphous	SiO_2	8–29	12
	SitGd amorphous	SiO_2–Gd_2O_3	6–29	18
	SitEu nanocrystalline	SiO_2–Eu_2O_3	8–40	15

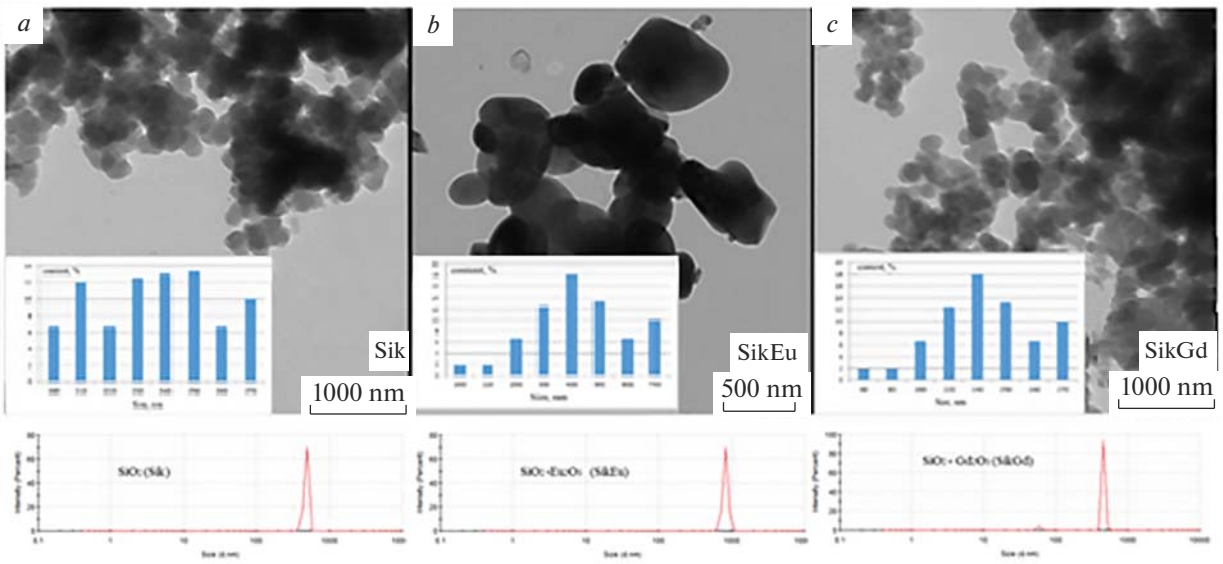

Fig. 3. The morphology determined by TEM and DLS of sample obtained according to the Scheme 1.

Morphology

The results of the morphology of samples are summarized in Table 2. The size of the particles obtained according to Scheme 1 is much greater than of the particles synthesized according to Scheme 2.

Samples of SiO_2 obtained according to the Scheme 1 (Fig. 3a) shows that the particles are spherical in shape, agglomerated, and their sizes are within the range of 200–270 nm as visible on the particle size distribution histogram. An average hydrodynamic radius of 450 nm determined using DLS method is higher than the radius determined by TEM. The actual measured hydrodynamic particle diameter (DLS) can be larger than the dry particle diameter (TEM), it is all a matter of a sample preparation. To perform DLS the nanoparticles were suspended in water making them hydrated, whereas for TEM the samples were dried on a grid. The use of two different and complementary methods provides an overall assessment of both particle size and morphology [37].

Results for SiO_2–Eu_2O_3 particles obtained according to the Scheme 1 (Fig. 3b) shows a changed shape of the particles – they are less rounded and the edges resemble the shape of a polygon. The dimensions are increased to 700 nm. The average hydrodynamic radius of 827 nm determined using the DLS method is also higher than the radius determined by TEM.

The image of round particles SiO_2–Gd_2O_3 obtained according to Scheme 1 (Fig. 3c) is similar to the image of silicon oxide particles. But the size distribution is different: 60–270 nm. The hydrodynamic sizes shows a bimodal distribution of the particles with peaks of 59 nm and 459 nm, which is formed typically by mixing particles with different growth mechanisms. That is, for the systems containing gadolinium oxide, the formation mechanism of silicon oxide particles and gadolinium oxide particles is different. This fact must be taken into account when creating a technology for the synthesis of compositions for various purposes based on the Gd_2O_3–SiO_2 system.

Particles of the materials obtained according to the Scheme 2 are nanoscale particles (Fig. 4). SiO_2 samples (Fig. 4a) are spherical in shape, agglomerated, and their sizes are in the range of 8–29 nm. The hydrodynamic radius – 12 nm (DLS) is within the radius determined by TEM.

Particles of SiO_2–Eu_2O_3 samples obtained according to the Scheme 2 (Fig. 4b) are oval-shaped nanoparticles, agglomerated, and their sizes are within the range of 8–40 nm. The average hydrodynamic radius is 15 nm. The point electronogram shows that the sample contains nanoparticles with crystalline ordering unlike the previously described particles where electronograms contain only halo rings typical of amorphous particles.

Figure 4c shows the SiO_2–Gd_2O_3 particles obtained using the Scheme 2. The nanoparticles are almost spherical particles with a diameter of 6–29 nm and an average hydrodynamic particle diameter of 18 nm. Spherical gadolinium oxide nanoparticles are distributed on the surface of silicon dioxide as visible on SEM image.

Note that the hydrodynamic size of the nanoparticles obtained according to the Scheme 2 is within the range of the particle sizes determined by TEM, which is due to the sample preparation technology. The fact is that an aqueous suspension of the material was prepared by ultrasonic treatment for 5 min. Apparently it destructed unstable agglomerates to nanosize, which

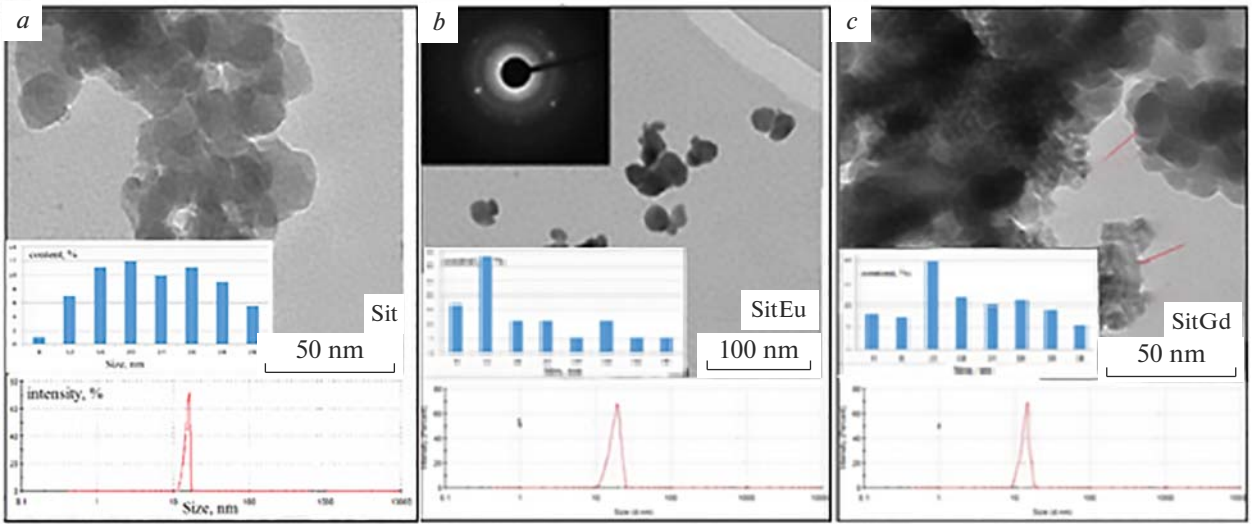

Fig. 4. The morphology determined by TEM and DLS of sample obtained according to the Scheme 2.

did not occur with the powders prepared according to the Scheme 1.

Luminescence Analysis

The luminescence spectrum in the Eu_2O_3–SiO_2 system synthesized according to the Scheme 1 (SikEu) consists of characteristic emission lines of the Eu^{3+} ion corresponding to electron transitions inside the 4f-shell (Fig. 5a). Each transition is split into two Stark lines: $^7F_1$–$^5D_1$ (541 and 545 nm); $^5D_0$–$^7F_1$ (587 and 594 nm); $^5D_0$–$^7F_2$ (619 and 622 nm); $^5D_0$–$^7F_3$ (647 and 652 nm); $^5D_0$–$^7F_4$ (698 and 702 nm). Moreover, an intense line $^5D_2$–$^7F_6$ (611 nm) is observed in the luminescence spectrum. Due to the presence of distortions in the Eu^{3+} crystal lattice, the electrodipole transition $^5D_0$–$^7F_2$ is more intense than the magnetic-dipole transition $^5D_0$–$^7F_1$. The ratio of the transition intensity $\eta = I(^5D_0$–$^7F_2)/I(^5D_0$–$^7F_1)$ is the criterion for the monochromaticity of the Eu^{3+} luminescence. High color purity is characterized by large values of η. In this study, η = 1.25. This value is small, indicating that the europium ion is intercalated in the silicate matrix, which causes the luminescence attenuation process.

The luminescence spectrum of the nanocrystalline sample obtained according to the Scheme 2 (SitEu) is shown in Fig. 5b. The difference in the spectra of the powder synthesized by different Schemes is manifested in the ratio of the supersensitive $^5D_0$–$^7F_2$ and magnetodipole $^5D_0$–$^7F_1$ transition bands. The value of η for SitEu increases up to 2.5. The sharp increase in the intensity of the supersensitive transition with respect to the magnetodipole transition indicates high symmetry of the coordination environment of the europium cation, as well as the formation of the nanocrystalline phase [38.

The luminescence spectrum in the Gd_2O_3–SiO_2 system synthesized according to the Scheme 1 (SikGd, Fig. 6a) consists of a broad band $^5D_0$–$^7F_4$ (700 nm) and two narrower bands $^7F_1$–$^5D_1$ (542 and 544 nm), $^5D_0$–$^7F_2$ (610 nm). For the nanopowder synthesized according to Scheme 2 (SitGd,

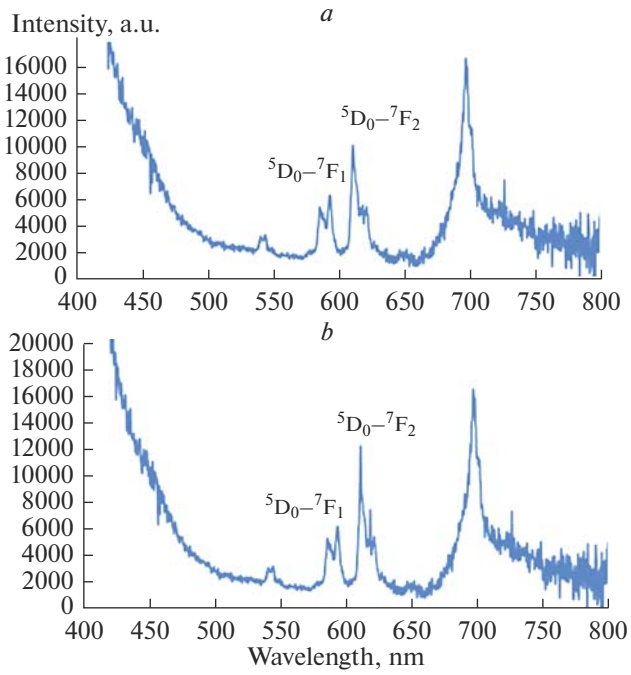

Fig. 5. Luminescence spectrum in the Eu_2O_3–SiO_2 system: a) synthesized according to Scheme 1; b) syn-thesized according to Scheme 2.

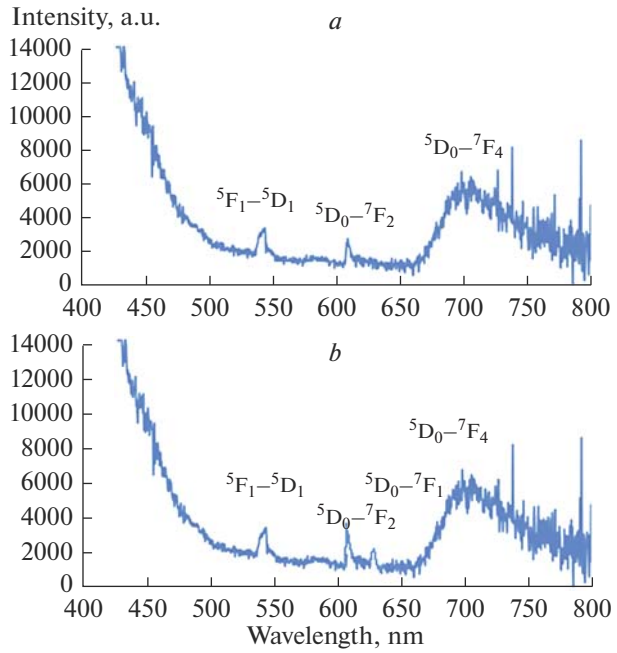

Fig. 6. Luminescence spectrum in the Gd_2O_3–SiO_2 system: (a) synthesized according to Scheme 1; (b) synthesized according to Scheme 2.

Fig. 6b) there is an increase in the intensity of $^5D_0$–$^7F_2$ (610 nm) and the appearance of a second $^5D_0$–$^7F_1$ peak (627 nm). As is well known, the luminescence intensity is determined, among other reasons, by the average distance between the luminescence centers. Obtaining of the nanoparticles according to Scheme 2 instead of microparticles synthesized by Scheme 2 is similar to the increasing of rare-earth atoms concentration in the silicate matrix resulting in a slight increase in luminescence.

CONCLUSIONS

Synthesis of the SiO_2, Gd_2O_3–SiO_2, Eu_2O_3–SiO_2 systems by two ways – using the silicon oxide isolated from kaolin and using the silicon oxide obtained by hydrolysis of tetraethoxysilane, allowed to obtain powders with different morphologies and luminescence properties. Using kaolin as starting material, results in particle size determined by DLS method (up to 450 nm for SiO_2 and Gd_2O_3–SiO_2 and 830 nm for Eu_2O_3–SiO_2) was significantly greater than that of the samples determined by TEM (270 nm for SiO_2 and Gd_2O_3–SiO_2 and up to 700 nm for Eu_2O_3–SiO_2), which is associated with the existence of a hydrated shell formed during sample preparation of powders for DLS. In case of tetraethoxysilane as initial substance for the synthesis of silicon oxide, the sample sizes determined by DLS and TEM methods are approximately the same if use the ultrasonic treatment (12–18 nm for DLS and 6–40 nm for TEM). Only sample of Eu_2O_3–SiO_2, synthesized using tetraethoxysilane is nanocrystalline (8–40 nm), all others are X-ray amorphous. The nanocrystallinity is also evidenced by a sharp increase in the intensity of the supersensitive transition with respect to the magnetodipole transition in the luminescence spectrum of the Eu_2O_3–SiO_2 sample compared with that obtained according to another way.

In the luminescence spectrum of the Gd_2O_3–SiO_2 nanopowder synthesized using tetraethoxysilane compared to that obtained using the kaolin, the intensity of $^5D_0$–$^7F_2$ increases and a second peak of $^5D_0$–$^7F_1$ appears. The increase of luminescence is a result of the obtaining of nanoparticles using tetraethoxysilane compared to microparticles obtained using the kaolin.

Finally, the results of this study demonstrate the ability to control the morphology and properties of SiO_2 – rare earth oxide systems not only by way of synthesis, but also by the choice of starting materials for silicon oxide.

ACKNOWLEDGMENTS

The results of the research were partially obtained using the equipment of the Centre for Collective Use of Scientific Equipment (CCUSE) at Voronezh State University (VSU).

CONFLICT OF INTEREST

The authors declare that they have no conflicts of interest.

REFERENCES

1. Thapa, R., Nissinen, T., Turhanen, P., Määttä, J., Vepsalainen, J., Lehto, V.-P., and Riikonen, J., Bisphosphonate modified mesoporous silicon for scandium adsorption, *Microporous Mesoporous Mater.,* 2020, vol. 296, p. 109980.
2. Toropov N.A., Bondar I.A., lazarev A.N., Smolin Yu.I. Silicates of rare earth elements and their analogues. *Publishing house "Science"*. leningrad. Otd., 1971, 230 p.
3. Yang, G., Yang, H., Zhang, X., Lqbal, K., Feng, F., Ma, J., Qin, J., Yuan, F., Cai, Y., and Ma, J., Surfactant-free self-assembly to the synthesis of MoO_3 nanoparticles on mesoporous SiO_2 to form MoO_3/SiO_2 nanosphere networks with excellent oxidative desulfurization catalytic performance, *J. Hazard. Mater.,* 2020, vol. 397, no. 14, p. 122654.
4. Khudhair, A.A., Bouchmella, K., Dorin, A.R., Mehdi, A., Mutin, P., and Hubert, H.V., One-step non-hydrolytic sol-gel synthesis of mesoporous SiO_2-Al_2O_3-NiO catalysts for ethylene oligomerization, *Microporous Mesoporous Mater.,* 2021, vol. 322, p. 111165.
5. Laskowska, M., Kityk, I., Pastukh, O., Dulski, M., Zubko, M., Jedryka, Ja., Cpałka, K., Zieliński, P.M., and Laskowski, Ł., Nanocomposite for photonics - nickel pyrophosphate nanocrystals synthesised in silica

nanoreactors, *Microporous Mesoporous Mater.,* 2020, vol. 306, no. 11, p. 110435.

6. Lenshin, A.S., Kashkarov, V.M., Spivak, Yu.M., and Moshnikov, V.A., Investigations of nanoreactors on the basis of p-type porous silicon: Electron structure and phase composition, *Mater. Chem. Phys.,* 2012, vol. 135, nos. 2–3, pp. 293–297.
7. Maniya, N.H. and Srivastava, D.N., Fabrication of porous silicon based label-free optical biosensor for heat shock protein 70 detection, *Mater. Sci. Semicond. Proces.,* 2020, vol. 115, p. 105126.
8. Weiss, S.M., Rong, G., and Lawrie, J.L., Current status and outlook for silicon-based optical biosensors, *Phys. E* (Amsterdam, Neth.), 2009, vol. 41, no. 6, pp. 1071–1075.
9. Daund, V., Chalke, S., Sherje, A.P., and Kale, P.P., ROS responsive mesoporous silica nanoparticles for smart drug delivery: A review, *J. Drug Deliv. Sci. Technol.,* 2021, vol. 64, p. 102599.
10. Zhu, H., Zheng, K., and Boccaccini, A.R., Multifunctional silica-based mesoporous materials for simultaneous delivery of biologically active ions and therapeutic biomolecules, *Acta Biomater.,* 2021, vol. 129, pp. 1–17.
11. Costa, J.A.S., de Jesus, R.A., Santos, D.O., Neris, J.B., Figueiredo, R.T., and Paranhos, C.M., Synthesis, functionalization, and environmental application of silica-based mesoporous materials of the M41S and SBA-n families: A review, *J. Environ. Chem. Eng.,* 2021, vol. 9, no. 3, p. 105259.
12. Wang, W., Zhao, W., Zhang, H., Xu, J., Zong, Li., Kang, Y., and Wang, A., Mesoporous polymetallic silicate derived from naturally abundant mixed clay: A potential robust adsorbent for removal of cationic dye and antibiotic, *Powder Technol.,* 2021, vol. 390, pp. 303–314.
13. Majeed, M.K., Saleem, A., Ma, X., and Ma, W., Clay-derived mesoporous Si/rGO for anode material of lithium-ion batteries, *J. Alloys Compd.,* 2020, vol. 848, p. 156590.
14. Han, X., Wang, Ya., Zhang, Na., Meng, J., Li, Ya., and Liang, J., Facile synthesis of mesoporous silica derived from iron ore tailings for efficient adsorption of methylene blue, *Colloids Surf., A,* 2021, vol. 617, p. 126391.
15. Zulfiqar, U., Subhani, T., and Husain, S.W., Synthesis and characterization of silica nanoparticles from clay, *J. Asian Ceram. Soc.,* 2016, vol. 4, pp. 91–96.
16. Wisser, F.M., Abele, M., Gasthauer, M., Muller, K., Moszner, N., and Kickelbick, G., Detection of surface silanol groups on pristine and functionalized silica mixed oxides and zirconia, *J. Colloid Interface Sci.,* 2012, vol. 374, pp. 77–82.
17. Darmakkolla, S.R., Tran, H., Guptaa, A., and Rananavare, Sh.B., A method to derivatize surface silanol groups to Si-alkyl groups in carbon-doped silicon oxides, *RSC Adv.,* 2016, vol. 6, pp. 93219–93230.
18. Maseme, M.R., Buitendach, B.E., Erasmus, E., and Swarts, J.C., The chemistry of spin-coated rhodium-ferrocenyl complexes supported on silanol-capped silicon wafers, *Polyhedron,* 2021, vol. 204, p. 115277.
19. Pavan, C., Turci, F., Tomatis, M., Ghiazza, M., Lison, D., and Fubini, B., Z potential evidences silanol heterogeneity induced by metal contaminants at the quartz surface: Implications in membrane damage, *Colloids Surf., B,* 2017, vol. 157, pp. 1449–455.
20. Zhang, R., Hua, M., Liu, H., and Li Jing, How to design nanoporous silica nanoparticles in regulating drug delivery: Surface modification and porous control, *Mater. Sci. Eng. B,* 2021, vol. 263, p. 114835.
21. Guo, J., Zhai, W., Sun, Q., Ai, Q., Li, J., Cheng, J., Dai, L., and Ci, L., Facilely tunable core-shell sisiox nanostructures prepared in aqueous solution for lithium ion battery anode, *Electrochim. Acta,* 2020, vol. 342, p. 136068.
22. Jung, Y., Huh, Y., and Kim, D., Recent advances in surface engineering of porous silicon nanomaterials for biomedical applications, *Microporous Mesoporous Mater.,* 2021, vol. 310, p. 110673.
23. Kozlova, S.A., Parfenov, V.A., Tarasova, L.S., and Kirik, S.D., The state of silanol coverage of the mesostructured silicate material MCM-41 as a result of post-synthetic activation, *J. Sib. Fed. Univ., Chem.,* 2008, vol. 41, pp. 376–388.
24. Gong, J., Lu, T., Xu, Z., Yin, J., Shao, H., and Wang, J., Light-assisted synthesis of copper/cuprous oxide reinforced nanoporous silicon microspheres with boosted anode performance for lithium-ion batteries, *Electrochim. Acta,* 2021, vol. 388, p. 138546.
25. Song, Y., Zhao, Zh., Li, J., You, Ya., Ma, X., Li, J., and Cheng, X., Preparation of silicon-doped ferrihydrite for adsorption of lead and cadmium: Property and mechanism, *Chin. Chem. Lett.,* 2021, vol. 32, no. 10, pp. 3169–3174.
26. Wu, N.-n., Wang, Ya-l., Liu, R.-t., Liu, H.-f., Liu, R., Li, A-x., and Xiong, X., Preparation and synthesis mechanism of ytterbium monosilicate nano-powders by a cocurrent coprecipitation method, *Ceram. Int., Part A,* 2020, vol. 46, no. 10, pp. 15003–15012.
27. Hafner, Th., Torvisco, A., and Uhlig, F., Building blocks for oligomeric siloxanes -selective chlorination of hydrido-siloxanes, *J. Organomet. Chem.,* 2018, vol. 875, pp. 1–4.
28. Lassalle, S., Jabbour, R., Del Rosal, I., Maron, L., Fonda, E., Veyre, L., Gajan, D., Lesage, A., Thieuleux, Ch., and Camp, Cl., Stepwise construction of silica-supported tantalum/iridium heteropolymetallic catalysts using surface organometallic chemistry, *J. Catal.,* 2020, vol. 392, pp. 287–301.
29. Lin, Yu-Sh., Hung, Y., Su, J.-K., Lee, R., Chang, Ch., Lin, M.-L., and Mou, Ch.-Yu., Gadolinium-mesoporous silica as a potential magnetic resonance imaging contrast agent, *Orient. J. Chem.,* 2018, vol. 34, no 5, pp. 2603–2607.
30. Ilves, V.G., Murzakaev, A.M., and Sokovnin, S., Yu, On the interrelationship of porosity and structural defects in amorphous-crystalline nanopowders SiO_2-doped Gd_2O_3 with their magnetic and luminescent properties, *Microporous Mesoporous Mater.,* 2018, vol. 271, pp. 203–218.
31. Ahlawat, R., Rani, N., and Goswami, B., Synthesis and characterizations of Eu_2O_3 nanocrystallites and its effect on optical investigations of Eu^{3+}, Eu^{2+}: SiO_2 nanopowder, J. Alloys Compd., 2018, vol. 743, pp. 126–135.

32. Aldalbahi, A., Mostafizur, R., and Anees, A., Mesoporous silica modified luminescent Gd_2O_3:Eu nanoparticles: Physicochemical and luminescence properties, *J. Sol-Gel Sci. Technol.,* 2019, vol. 89, no. 3, pp. 785–795.

33. Millán, A.J., Moreno, R., and Nieto, M.I., Thermogelling polysaccharides for aqueous gelcasting. Part I: A comparative study of gelling additives, *J. Eur. Ceram. Soc.,* 2002, vol. 22, pp. 2209–2215.

34. Luz, A.P., Moreira, M.H., Braulio, M.A.L., Parr, C., and Pandolfelli, V.C., Drying behavior of dense refractory ceramic castables. Part 1 - General aspects and experimental techniques used to assess water removal, *Ceram. Int.,* 2021, vol. 47, no. 16, pp. 22246–22268.

35. Abdelwahed, W., Degobert, Gh., Stainmesse, S., and Hatem, F., Freeze-drying of nanoparticles: Formulation, process and storage considerations, *Adv. Drug Deliv. Rev.,* 2007, vol. 58, no. 15, pp. 1688–1713.

36. Nimesh, S., *Gene Therapy: Potential Applications of Nanotechnology,* London: Woodhead, 2013.

37. Medina-Velazquez, D.Y., Barraza, M., Barron, M., Hileio, I., and Colin, V., Influence of synthesis parameters on luminescence of thenoyltrifluoroacetone europium powders, *J. Mater. Sci. Chem. Eng.,* 2018, vol. 6, no. 8, pp. 1–8.

SPELL: 1. OK